11th International Conference on Electrical, Electronics and Computer Engineering (IcETRAN), Nis, 3-6 June 2024

Design of $Ga_2O_3/(AlGa)_2O_3$ Double-Barrier Resonant Tunnelling Diode

Novak Stanojević
School of Electrical Engineering
University of Belgrade
Vlatacom Institute of High Technologies
Belgrade, Serbia
novak.stanojevic@vlatacom.com
0009-0007-5122-2219

Aleksandar Demić
School of Electronic and Electrical Engineering
University of Leeds
Leeds, United Kingdom
A.Demic@leeds.ac.uk
0000-0003-1335-6156

Xizhe Wang
School of Electronic and Electrical Engineering
University of Leeds
Leeds, United Kingdom
el17xw@leeds.ac.uk

Nikola Vuković
School of Electrical Engineering
University of Belgrade
Belgrade, Serbia
nvukovic@etf.bg.ac.rs
0000-0002-4941-2546

Dragan Indjin
School of Electronic and Electrical Engineering
University of Leeds
Leeds, United Kingdom
D.Indjin@leeds.ac.uk
0000-0002-9121-9846

Jelena Radovanović
School of Electrical Engineering
University of Belgrade
Belgrade, Serbia
radovanovic@etf.bg.ac.rs
0000-0003-3031-7802).

2024 11th International Conference on Electrical, Electronic and Computing Engineering (IcETRAN) | 979-8-3503-8699-8/24/$31.00 ©2024 IEEE | DOI: 10.1109/ICETRAN62308.2024.10645113

***Abstract*— In this work, we calculate for the first time the electronic structure, current-density-voltage characteristic and transmission spectrum of novel $Ga_2O_3/(AlGa)_2O_3$ double-barrier resonant tunnelling diodes (RTDs). The performance of RTDs were optimised in terms of barrier thickness and doping level for maximum peak-to-valley ratio and a maximal value of 3.87 was predicted. The simulations also show that the optimal barrier thickness of the analysed $Ga_2O_3/(Al_{12}Ga_{88})_2O_3$ double-barrier RTD is 1.6 nm and the optimal doping level is around $8 \cdot 10^{17}$ cm^{-3}. RTDs are considered due to their importance for design of wide-bandgap oxide semiconductor structures with an optimized resonant electron transport mechanism which is of particular interest in designing novel wide-gap oxide-based quantum cascade lasers.**

Keywords*— *Wide-bandgap oxide semiconductors; resonant tunnelling, negative differential resistance

I. Introduction

Double barrier resonant-tunneling diodes (RTDs) are multi-layer semiconductor structures consisting of a single quantum well surrounded by thin barrier layers. They make use of quantum mechanical resonant tunneling of electrons through the barrier layers into the quasi-bound states of the quantum well, resulting in the presence of one or more negative differential resistance (NDR) regions in the current–voltage characteristic which enables many unique applications. Due to the very fast electron tunneling through the thin barrier layers, these diodes are capable of ultra-high-speed operation having applications in oscillator construction and switching devices operating at terahertz frequencies [1].

RTDs can be fabricated from many different material systems, such as III–V, IV and II–VI type semiconductors. Due to their large conduction-band energy discontinuity $Ga_2O_3/(AlGa)_2O_3$ [2] and ZnO/ZnMgO [3, 4] are promising candidates for high operating temperature and power output terahertz (THz) frequency oscillators. In recent years a significant amount of research has been devoted to investigation of $Ga_2O_3/(AlGa)_2O_3$ material parameters, processing, and doping [5-8]. Furthermore, RTD design and construction is an important step for the design and construction of THz quantum cascade lasers - unipolar semiconductor lasers with tuneable emission wavelengths that can be engineered by variation of semiconductor layer thicknesses [9,10]. Moreover, terahertz radiation has attracted much attention due to the increasing number of possible applications in medical diagnostics, chemical sensing, and imaging [11-18].

In this work, we numerically investigate the $Ga_2O_3/(Al_{12}Ga_{88})_2O_3$ double-barrier RTD and optimise the design in terms of barrier thickness and doping density for maximum peak-to-valley ratio (PVR).

II. Theoretical Model

For calculating the electronic structure of a RTD, just as for any semiconductor quantum well system we start from the one-dimensional effective-mass envelope function Schrödinger equation:

$$-\frac{\hbar^2}{2}\frac{d}{dz}\frac{1}{m^*(z)}\frac{d\psi(z)}{dz}+U_{eff}(z)\psi(z)=E\psi(z) \quad (1)$$

where m^* is the effective mass of the electron along the growth direction, which varies with position due to the changes in material composition. E is the electron energy, $\psi(z)$ is the envelope wave function, and $U_{eff}(z)$ is the total effective potential energy given as:

$$U_{eff}(z)= U_c(z)-e\varphi(z)-eF_e z \quad (2)$$

where $U_c(z)$ is the conduction band offset of the heterostructure, $\varphi(z)$ is electrostatic potential, and F_e is the externally applied electric field.

The electrostatic potential is calculated from the Poisson equation:

$$\frac{d^2\varphi(z)}{dz^2}=\frac{e}{\varepsilon(z)}\big(n(z)-N_D(z)\big) \quad (3)$$

This work was supported by the Vlatacom Institute of High Technologies under project 178, Ministry of Science, Technological Development and Innovation of the Republic of Serbia under contract number: 451-03-65/2024-03/200103, "Multi-Scale Modeling of Terahertz Quantum Cascade Laser Active Regions", Multilateral scientific and technological cooperation in the Danube region 2020-2021, DEMETRA: Development of high-performance mid-IR / THz quantum cascade lasers for advanced applications", Science Fund of the Republic of Serbia, Serbian Science and Diaspora Collaboration Programme: Knowledge Exchange Vouchers, Science Fund of the Republic of Serbia, Grant #10504, Ultra-short pulsations from TERAhertz quantum cascade laser using passive mode-LOCKing with graphene saturable absorber – TERALOCK, European Cooperation in Science and Technology (COST) Action CA21159 PhoBioS

where $\varphi(z)$ is the electrostatic potential, $n(z)$ the electron density, $N_D(z)$ the doping concentration, and $\varepsilon(z)$ the dielectric constant.

In the case of potential barrier-based structures, such as RTDs, all of the electron energy states belong to a continuum spectrum, whereas the resonant electron states can be described by the transmission (tunnelling) coefficient $\tau(E)$.

We can approximately express the electron density $n(z)$ in the resonant tunnelling structure as [19,20]:

$$n(z) = \frac{k_B T}{2^{\frac{3}{2}}\pi^2\hbar^3}\left(\int_{E_c}^{\infty} |\psi(z,E)|^2 (m^*)^{\frac{3}{2}} E^{-\frac{1}{2}} \ln\left[1 + e^{\frac{(E_F - E)}{k_B T}}\right] + \int_{E_c - eV_R}^{\infty} |\psi(z,E)|^2 (m^*)^{\frac{3}{2}} E^{-\frac{1}{2}} \ln\left[1 + e^{\frac{(E_F - E - eV_R)}{k_B T}}\right]\right) dE \quad (4)$$

where the reference level E_c is the conduction band minima, and m^* is the effective mass in well material. The potential drop along the structure V_R is calculated using the length of the resonant structure l as $V_R = F_e \cdot l$. The Fermi energy in the highly doped emitter/collector of RTD E_F is calculated using Fermi-Dirac statistics under the assumption that all of the donors are ionized, resulting in $n(z) = N_D$ in the emitter/collector [21].

The total effective potential energy is a function of the electrostatic potential (2), which depends on the electron density (3) calculated as in equation (4) from the envelope functions found from the Schrödinger equation (1). For this reason this system of Schrödinger-Poisson equations needs to be solved self-consistently.

The resonant-tunneling current density for an applied terminal voltage can be calculated using the Esaki-Tsu formula [22].

$$J = \frac{e k_B T}{2\pi^2\hbar^3} \int_{E_c}^{\infty} m^* \tau(E) \ln\left[\frac{1 + e^{\frac{E_F - E}{k_B T}}}{1 + e^{\frac{E_F - E - eV_R}{k_B T}}}\right] dE \quad (5)$$

This is a simplified approach that assumes a coherent picture of electron tunnelling in which electron transport is not affected by any scattering effects that break phase coherence [19]. This carrier transport model is often used for characterization of resonant tunnelling structures made of different materials [19, 20, 23]. The current density obtained from (5) does not take into account the scattering current and the thermionic current and as a result, should be used for approximate calculations of electron transport and identifying and predicting negative differential resistivity behavior..

III. Results and Discussion

In this section, we present the results of our numerical simulations. In order to show the sensitivity of the RTD performance on the thickness of the barrier layers and doping density we start our analysis with a double-barrier resonant tunnelling structure with two $(Al_{12}Ga_{88})_2O_3$ barrier layers being 1.5 nm thick surrounding the 4 nm thick Ga_2O_3 well layer. The parameters of the barrier layers (thickness and Al composition) were chosen to resemble the resonant tunnelling part of a prospective QCL structure. The double barrier structure is located between the Ga_2O_3 emitter and collector region whose Sn doping was set to $N_D = 1 \cdot 10^{18}$ cm^{-3}. The voltage V_R across the structure was varied between 0 and 0.25V. The values of the electron effective mass, dielectric constant of both Ga_2O_3 and $(Al_{12}Ga_{88})_2O_3$ as well as the conduction band offset between these two materials used in the simulations were the same as in [5]

The band structure and electron concentration was solved self-consistently at T=300K, and the results for three different applied voltages are shown in Fig. 1.

It can be seen how the conduction-band edge bends due to the applied voltage. With the increase of the applied voltage, the conduction-band edge bends more and the electron concentration in the emitter region is increased, which results in a stronger self-consistent field resulting in larger band bending in the emitter region ($V_R = 0.2$ V).

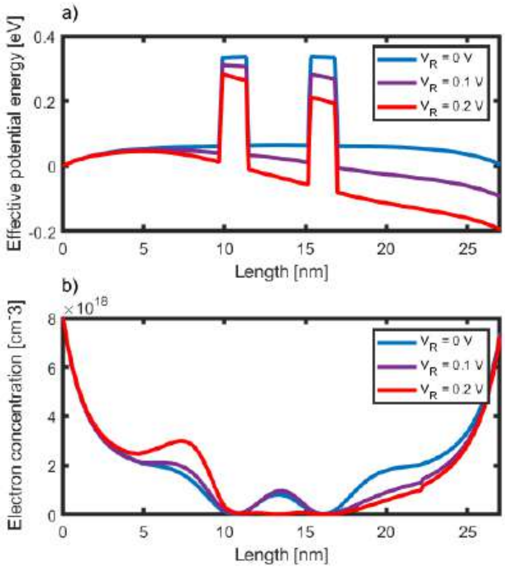

Fig. 1. Self-consistent potential energy and corresponding electron concentration in an examplar $Ga_2O_3/(AlGa)_2O_3$ RTD for three different applied voltages.

To analyse the effect of layer thickness fluctuation in a $Ga_2O_3/(Al_{12}Ga_{88})_2O_3$ double-barrier RTD we calculate the current-density – voltage characteristic while varying the thickness of both barrier layers from 0.5 nm to 2.5 nm.

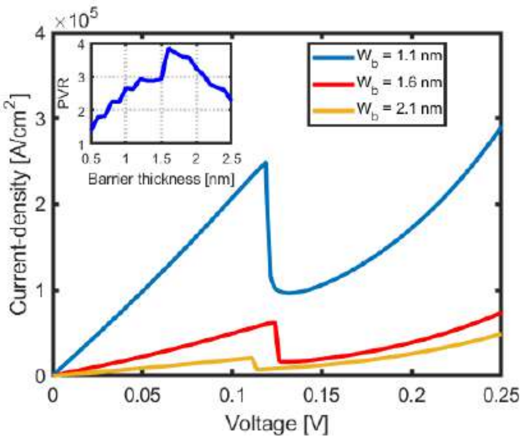

Fig. 2. Current-density - voltage characteristics of $Ga_2O_3/(Al_{12}Ga_{88})_2O_3$ double-barrier RTD for three different barrier layer thickness values. The inset shows the current-density peak-to-valley (PVR) ratio at NDR as a function of the barrier thickness. The doping density value in the emitter/collector was $1 \cdot 10^{18}$ cm^{-3}.

For each RTD in this simulation set, we calculate the PVR of the current density at NDR in order to find the optimal barrier thickness. The peak-to-valley ratio is the ratio between the maximum and minimum value of the current density around the NDR points in the current-density – voltage characteristic.

Depending on the design of the electron bound states in the quantum well RTDs can have multiple NDR regions, but the first NDR region is the most important for practical applications.

The variation in the barrier thickness results in a significant change in the tunneling current. While the current density increases with the decrease of the barrier thickness the inset in Fig. 2. shows that the optimal barrier thickness, in terms of the PVR, is equal to 1.6 nm. For this reason, in Fig. 2. we show the current-density – voltage characteristics for both barrier layers equal to 1.6 nm, as well as reasonable barrier thickness values of 1.1 nm and 2.1 nm. The doping density value in the emitter/collector was 10^{18} cm^{-3} . For this optimal barrier thickness of 1.6 nm, the PVR is ~ 3.85. In all following simulations we use this optimal barrier thickness value.

In order to analyse the effect of doping density variation in a $Ga_2O_3/(Al_{12}Ga_{88})_2O_3$ double-barrier RTD we calculate the current-density – voltage characteristic while varying the doping level in the emitter and collector region from $1 \cdot 10^{17}$ cm^{-3} to $5 \cdot 10^{18}$ cm^{-3}. For each RTD in this simulation set, we calculate the PVR of the current density at NDR in order to find the optimal doping level.

Fig. 3. shows the current-density – voltage characteristics for the doping level in the emitter and collector region equal to $3 \cdot 10^{17}$ cm^{-3}, $8 \cdot 10^{17}$ cm^{-3} and $3 \cdot 10^{18}$ cm^{-3}. The variation in the doping level results in a significant change in the tunneling current due to a larger number of carriers. While the current density increases with the increase of the doping level the inset shows that the optimal doping level, in terms of the PVR, is equal to $8 \cdot 10^{17}$ cm^{-3}. For this doping level the PVR is ~ 3.87. In all following simulations, we use this optimal doping level value as well as the optimal barrier thickness as these parameters result in an optimal RTD with the largest PVR.

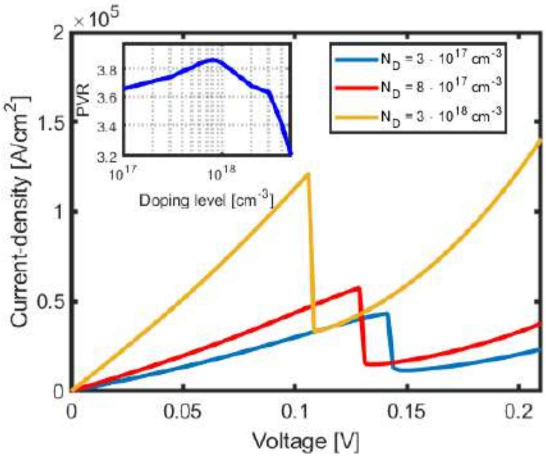

Fig. 3. Current-density - voltage characteristics of $Ga_2O_3/(Al_{12}Ga_{88})_2O_3$ double-barrier RTD for three different doping level values. The inset shows the current-density peak-to-valley (PVR) ratio at NDR as a function of the doping level. The thickness of both barrier layers was 1.6 nm.

To better understand the nature of the NDR region in an RTD in Fig. 4 we show the bottom of the conduction band of the optimal RTD for the applied voltage at NDR (VNDR = 0.1288 V). This is shown as the blue line, whilst the band diagram for no applied voltage is shown by the red line. The yellow and orange lines denote the wave functions squared for the first and second bound state of the quantum well respectively at the NDR voltage. The green line represents the Fermi energy of the emitter region.

For no applied voltage the Fermi energy is below the first bound state, and as the voltage increases the first bound state of the quantum well lowers and is closer to the Fermi level, so the current it carries increases which corresponds to the region to the left of the NDR region in Fig. 3 (red line). The current reaches a local maximum for the beginning of the NDR region VNDR = 0.1288 V (which can be seen in Fig. 3. as the local maxima of the red line).

For this applied voltage the energy of the first bound state is equal to the Fermi energy of the emitter region which can be seen in Fig. 4. The transmission coefficient of the quantum well has a peak value for this energy, which can be seen in the transmission spectrum in Fig. 5., and the current reaches a maximal value.

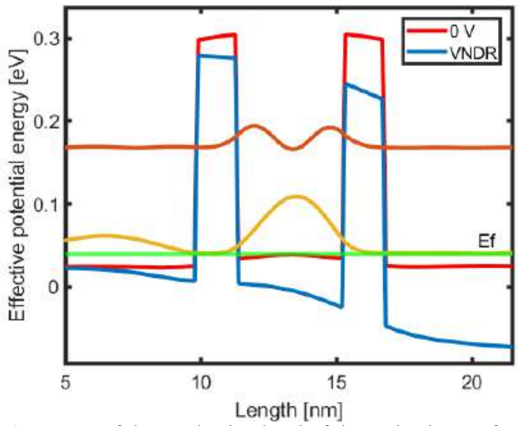

Fig. 4. Bottom of the conduction band of the optimal RTD for the applied voltage VNDR = 0.1288 V (blue line) and no applied voltage (red line). The wave functions squared for the first (yellow line) and second (range line) bound state of the quantum well and the Fermi energy of the emitter region (green line) for the applied voltage VNDR are shown.

Increasing the applied voltage lowers the first bound state which gradually enters the energy bandgap range, and as a result, no longer carries any current. For these voltages, the second bound state is high above the Fermi energy and does not conduct significant current and this corresponds to the NDR region. Further increase of the applied voltage lowers the second bound state of the quantum well making it closer to the Fermi energy of the emitter region so the current it carries increases, which corresponds to the region to the right of the NDR region in Fig. 3 (red line).

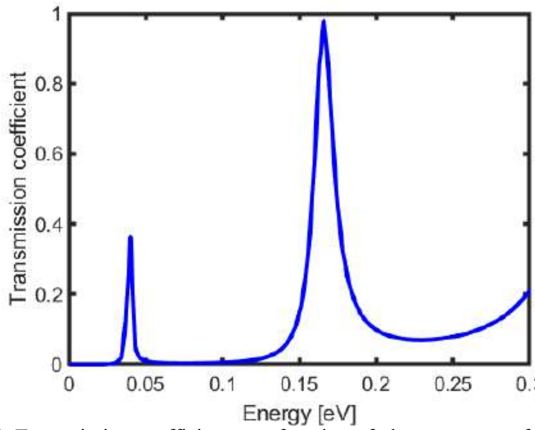

Fig. 5. Transmission coefficient as a function of electron energy for an NDR voltage of 0.1288 V applied on a $Ga_2O_3/(Al_{12}Ga_{88})_2O_3$ double-barrier RTD with the optimal barrier thickness of 1.6 nm and the optimal doping level of $8 \cdot 10^{17}$ cm^{-3}.

We have designed an optimised $Ga_2O_3/(Al_{12}Ga_{88})_2O_3$ double-barrier RTD with a maximal PVR ratio of 3.87. Previous results have reported a PVR of 2 for a RTD grown from $Ga_2O_3/(Al_{15}Ga_{85})_2O_3$ [2], the PVR of 2.9 for a Si/SiGe RTDs [24], while the maximum PVR for GaAs/AlAs [25] and InGaAs/AlAs [26] RTDs were 3.9 and 14 respectively. All of these values are given for operation at room temperature.

IV. Conclusion

In this work we have analysed $Ga_2O_3/(Al_{12}Ga_{88})_2O_3$ double-barrier resonant tunneling diodes, structures which have not been numerically simulated in detail in the literature. We have calculated their electronic structure, current-density-voltage characteristic and transmission spectrum.

Our results show that the current density PVR is sensitive to both barrier thickness variation and changes of doping level of the emitter and collector region. We have designed an optimised RTD with a maximal PVR of ~ 3.87 for a barrier thickness of 1.6 nm and doping level of $8 \cdot 10^{17}\ \mathrm{cm}^{-3}$. This is an important step as it shows the possibility of efficient tunneling transport through thin $(Al_{12}Ga_{88})_2O_3$ layers. The presented work, together with prospective calculation of optical absorption in multi-quantum well structures, is the building block for the design and prospective demonstration of $Ga_2O_3/(Al_{12}Ga_{88})_2O_3$ THz quantum cascade lasers.

References

[1] D. Saeedkia, Handbook of Terahertz Technology for Imaging, Sensing and Communications. Elsevier. p. 429 (2013).

[2] O. Hironori Growth of double-barrier β-$(AlGa)_2O_3/Ga_2O_3$ structure and heavily Sn-doped Ga_2O_3 layers using molecular-beam epitaxy Jpn. J. Appl. Phys. **59** 075503 (2020).

[3] V.P. Sirkeli, S.A. Vatavu, O. Yilmazoglu, S. Preu, H.L. Hartnagel, Negative Differential Resistance in ZnO-Based Resonant Tunneling Diodes. In Proceedings of the 2019 44th International Conference on Infrared, Millimeter, and Terahertz Waves; IEEE, p. 1–2 (2019).

[4] A. Atić, X. Wang, N. Vuković, N. Stanojević, A. Demić, D. Indjin, J. Radovanović, Resonant Tunnelling and Intersubband Optical Properties of ZnO/ZnMgO Semiconductor Heterostructures: Impact of Doping and Layer Structure Variation, Materials **17**, no. 4, 927 (2024).

[5] J. E. Lyman, S. Krishnamoorthy, Theoretical investigation of optical intersubband transitions and infrared photodetection in β-$(Al_xGa_{1-x})_2O_3/Ga_2O_3$ quantum well structures, Journal of Applied Physics, **127** (17) (2020).

[6] S. J. Pearton, J. Yang, P. H. Cary IV, F. Ren, J. Kim, M. J. Tadjer, M. A. Mastro, A review of Ga2O3 materials, processing, and devices, Appl. Phys. Rev. **5**, 011301 (2018).

[7] J. Zhang, J. Shi, D. C. Qi, L. Chen, K. H. Zhang, Recent progress on the electronic structure, defect, and doping properties of Ga_2O_3. APL Materials, **8** (2). (2020).

[8] J. B. Varley, A. Perron, V. Lordi, D. Wickramaratne, J. L. Lyons, Prospects for n-type doping of $(Al_xGa_{1-x})_2O_3$ alloys. Applied Physics Letters, **116** (17) (2020).

[9] J. Faist, F. Capasso, D. L. Sivco, C. Sirtori, A. L. Hutchinson, and A. Y.Cho, Quantum cascade laser, Science **264**, 553 (1994).

[10] R. Köhler, A. Tredicucci, F. Beltram, H. E. Beere, E. H. Linfield, A. G. Davies, D. A. Ritchie, R. C. Iotti and F. Rossi, Terahertz semiconductor-heterostructure laser. Nature **417**, 156–159 (2002).

[11] C. Gmachl, F. Capasso, D. L. Sivco, and , A. Y. Cho, Recent progress in quantum cascade lasers and applications. Rep. Prog. Phys. **64**,1533 (2001).

[12] A. A. Kosterev, and F. K. Tittel, Chemical sensors based on quantum cascade lasers. IEEE J. Quantum Electron. **38**, 582–591 (2002).

[13] G. Wysocki, R. Lewicki, R.F. Curl, F.K. Tittel, L. Diehl, F. Capasso, M. Troccoli, G. Hofler, D. Bour, S. Corzine, R. Maulini, M. Giovannini & J. Faist, Widely tunable mode-hop free external cavity quantum cascade lasers for high resolution spectroscopy and chemical sensing. Appl. Phys. B **92**, 305–311 (2008).

[14] J.B. McManus, J.H. Shorter, D.D. Nelson, M.S. Zahniser, D.E. Glenn & R.M. McGovern, Pulsed quantum cascade laser instrument with compact design for rapid, high sensitivity measurements of trace gases in air. Appl. Phys. B **92**, 387 (2008).

[15] P. Dean, A. Valavanis, J. Keeley, K. Bertling, Y. L. Lim, R. Alhathloo, A. D. Burnett, L. H. Li, S. P. Khanna, D. Indjin, T. Taimre, A. D. Rakić, E. H. Linfield and A. G. Davies, Terahertz imaging using quantum cascade lasers-a review of systems and applications. J. Phys. D Appl. Phys. **47**, 374008 (2014).

[16] P. Dean, O. Mitrofanov, J. Keeley, I. Kundu, L. Li, E. H. Linfield, A. G. Davies, Apertureless near-field terahertz imaging using the self-mixing effect in a quantum cascade laser. Appl. Phys. Lett. **108**, 091113 (2016).

[17] A. D. Rakić, T. Taimre, K. Bertling, Y. L. Lim, P. Dean, D. Indjin, Z. Ikonić, P. Harrison, A. Valavanis, S. P. Khanna, M. Lachab, S. J. Wilson, E. H. Linfield, A. G. Davies, Swept-frequency feedback interferometry using terahertz frequency QCLs: A method for imaging and materialsanalysis. Opt. Express **21**, 22194–22205 (2013).

[18] Y. L. Lim, T. Taimre, K. Bertling, P. Dean, D. Indjin, A. Valavanis, S. P. Khanna, M. Lachab, H. Schaider, T. W. Prow, H. P. Soyer, S. J. Wilson, E. H. Linfield, A. G. Davies, and A. D. Rakić, High-contrast coherent terahertz imaging of porcine tissue via swept-frequency feedback interferometry. Biomed. Opt. Express **5**, 3981–3989 (2014).

[19] H. Mizuta, T. Tanoue, The Physics and Applications of Resonant Tunnelling Diodes; Cambridge University Press, (1995)

[20] M. Indjin, J. Griffiths, Coherent Electron Quantum Transport in In0.53Ga0.47As/GaA0.51Sb0.49 Double Barrier Resonant Tunnelling Structures. Opt. Quantum Electron. **52**, 265 (2020)

[21] J.S. Blakemore, Semiconducting and Other Major Properties of Gallium Arsenide. J. Appl. Phys. **53**, R123–R181 (1982)

[22] L.L. Chang, L. Esaki, R. Tsu, Resonant Tunneling in Semiconductor Double Barriers. Appl. Phys. Lett. **24**, 593–595 (1974)

[23] S. Sakr, E. Warde, M. Tchernycheva, F. H. Julien, Ballistic Transport in GaN/AlGaN Resonant Tunneling Diodes. J. Appl. Phys. **109** (2011)

[24] P. See, D. J. Paul, B. Hollander, S. Mantl, I. V. Zozoulenko and K. F. Berggren, High performance Si/Si/sub 1-x/Ge_x resonant tunneling diodes. IEEE Electron Device Letters, **22(4)**, 182-184 (2001)

[25] C. I. Huang, M. J. Paulus, C. A. Bozada, S. C. Dudley, K. R. Evans, C. E. Stutz, R. L. Jones and M. E. Cheney, AlGaAs/GaAs double barrier diodes with high peak-to-valley current ratio. Appl. Phys. Lett. **51(2)**, 121-123 (1987)

[26] T. Inata, S. Muto, Y. Nakata, S. Sasa, T. Fujii, S. Hiyamizu, A pseudomorphic In0.53Ga0.47As/AlAs resonant tunneling barrier with a peak-to-valley current ratio of 14 at room temperature, Jpn. J. Appl. Phys. **26** (Part 2, No. 8) L1332–L1334 (1987)